Hedgehog signalling and lipid metabolism in glia regulate neural stem cell proliferation in *Drosophila*

Qian Dong[1,2], Michael Zavortink[1,2], Francesca Froldi[1,2], Tammy Lam[1,2], Louise Y. Cheng[1,2,3]

1 Peter MacCallum Cancer Centre, 305 Grattan St, Parkville, Victoria, 3000

2 Sir Peter MacCallum Department of Oncology, University of Melbourne, Parkville, Victoria, Australia, 3010

3 The Department of Anatomy and Neuroscience, University of Melbourne, Parkville, Victoria, Australia, 3010

Email: louise.cheng@petermac.org

Telephone: +61 450053363

Summary:

The final size of the adult central nervous system (CNS) is determined by the size of neuronal lineages generated by neural stem cells (NSCs) during development. In *Drosophila*, NSCs called neuroblasts (NBs) reside within a specialised microenvironment called the glial niche. Here, we explore non-cell autonomous regulation of NB behaviour by glia during normal development, and upon glial overgrowth. We show that lipid droplets that reside within the glial niche are closely associated with the signalling molecule Hedgehog (Hh). Under physiological conditions, Hh is present at low levels in the glial niche to ensure NBs faithfully produce the correct number and types of progeny that populate the adult nervous system. Upon Fibroblast Growth Factor (FGF) activation in glia, an accumulation of lipid droplets and Hh ligand non-cell autonomously triggers adjacent NBs to reduce their cell cycle speed, increase the developmental period in which they proliferate and disrupt their asymmetric division. Downstream of FGF signalling in the glia, we found that lipid metabolism affects both Hh subcellular localisation, as well as Hh post-translational modification, to modulate its activity, and in turn, its ability to activate Hh-signalling in the adjacent NBs. Together, our data suggest that wildtype and dysfunctional glial niche non-autonomously regulate neural lineage size via modulation of lipid metabolism and Hedgehog signalling.

Keywords: Neuroblasts, Hh signalling, lipid droplets, glia

Introduction:

Neurogenesis occurs during development to build the adult nervous system directly or indirectly (via intermediate progenitors) from a population of asymmetrically dividing self-renewing and multipotent neural stem cells known as neuroblasts (NBs) (Homem and Knoblich, 2012). The vast majority of NBs are specified during embryogenesis, proliferate throughout larval development, and cease to proliferate during pupal stages. Type I NBs are located within the ventral nerve cord (VNC) and the central brain (CB), and are the predominant type of NBs, while type II NBs give rise to eight NB lineages located on the dorsal surface of the central brain. During each type I NB cell division, NBs self-renew, and produce a smaller ganglion mother cell (GMC) daughter that creates a limited numbers of neurons and/or glia. The ability of NBs to divide and generate appropriate progeny number and cell diversity is determined by their ability to maintain asymmetric division, regulate their cell cycle speed, and timely cell cycle entry/exit at the beginning and end of neurogenesis (Homem and Knoblich, 2012). Cell intrinsic mechanisms such as the temporal regulation of NB identity via transcription factors that are expressed throughout the life time of the NBs, impact on these characteristics (reviewed by (Doe, 2017). However, the contribution of the NB microenvironment, or niche, on the of the ability of NBs to build the nervous system is less well understood.

Stem cell niches are microenvironments that sustain their normal functions, including their cell division characteristics, differentiation and ability to integrate into circuits and perform appropriate function in the mature CNS (Bjornsson et al., 2015). In the *Drosophila* CNS, larval NBs reside in a niche that includes a variety of glial cells. The glial niche not only acts as scaffolds for neurons but are known to play more active roles to influence NB behavior. It encapsulates NBs and their recently born progeny, and produces Insulin-like peptide 6 (Dilp6) in response to feeding at early larval stages to reactivate the NB cell cycle (Chell and Brand, 2010; Sousa-Nunes et al., 2011), via activation of PI3K and inhibition of the Hippo signalling pathway (Ding et al., 2016; Poon et al., 2016). Furthermore, the expansion of glial membrane processes in response to nutrition is important for the survival of newly

born neuronal progeny (Speder and Brand, 2018). After NB entry into the cell cycle, the niche has been shown to be important for buffering the effects of environmental stress on the NBs. Under starvation conditions, the niche-derived signalling molecule Jellybelly allows the NBs to divide despite nutrient restriction (Cheng et al., 2011). More recently, lipid droplets residing within the glial niche were shown to protect NBs from peroxidation chain reactions induced by oxidation of polyunsaturated fatty acids (PUFAs) (Bailey et al., 2015). In a disease context, Reactive Oxidative Stress (ROS) and neuronal mitochondrial dysfunction causes an accumulation of lipid droplets in the adult glia; abolishing lipid droplet accumulation delays the onset of neurodegeneration in both flies and mammals (Liu et al., 2015; Marschallinger et al., 2020). However, secreted signals from the glial niche that are required to maintain NB proliferation under physiological conditions beyond the context of NB reactivation are so far unknown, and how dysfunction of the glial niche affects NB behaviour remains uncharacterised.

Here, we show that organelles called lipid droplets and the signalling molecule Hedgehog (Hh) are closely associated in cortex glial cells during larval neurogenesis. Glial niche derived Hh ligand is normally maintained at low levels, to limit the activation of Hh signalling in the NB, and promote its cell cycle progression. Hh levels and its ability to signal to NBs is regulated by 1) Lsd2, which modulates Hh subcellular localisation, and 2) via palmitoylation, a lipid-mediated post-translational modification that affects Hh's ability to carry out signal transduction. Upon glial niche expansion via FGF-activation, accumulation of Hh ligand activates Hh-signalling in the NB, which in turn inhibits their ability to undergo timely cell cycle exit, asymmetric self-renewal, and cell cycle progression. Together, our study shows that glial niche-derived Hh signals to NBs during physiological and diseased contexts, to regulate neural lineage size, and this signaling is modulated by lipid metabolism.

Results:

Glial FGF signalling alters cortex glial membrane volume and the ability of glia to enwrap NBs

A number of signalling pathways including PI3K, Hippo, EGFR and FGF are instrumental in mediating the growth and proliferation of glial cells during

neurogenesis (Avet-Rochex et al., 2012; Read et al., 2009; Reddy and Irvine, 2011; Witte et al., 2009). To investigate how the glial niche non-autonomously affects NB behaviour, we manipulated the size of the niche via activation or inhibition of the FGF signalling pathway (Avet-Rochex et al., 2012). Consistent with previous studies, we found that activation of glial FGF signalling via expression of an activated form of the FGF receptor heartless (htl^{ACT}), increased the volume of superficial (Figure1B-D) and cortex glial cells (Figure 1E-G). Conversely, down regulation of glial FGF signalling with a dominant negative form of Htl (htl^{DN}), reduced glial volume (Figure 1A, (Avet-Rochex et al., 2012). Concurrent with the start of glial proliferation (48hr After Larval Hatching - ALH), the glial cell membrane remodels to create discrete cortex glial chambers that separate NB lineages (Speder and Brand, 2018). We found that the amount of glial membrane that encloses each NB was significantly increased by glial-specific FGF activation and reduced via its inhibition (Figure 1H-K).

Glial FGF signalling non-autonomously affects NB behaviour

To assess how glia-derived signals affect the behaviour of neighbouring NBs, we assessed three key parameters: 1) the overall period of NB proliferation throughout CNS development; 2) the balance between NB self-renewal vs. differentiation as regulated by the asymmetric division machinery; and 3) NB cell cycle speed (Homem and Knoblich, 2012). Neurogenesis starts and stops in a spatial and temporally defined manner (Chell and Brand, 2010; Isshiki et al., 2001; Maurange et al., 2008; Sousa-Nunes et al., 2011). Consistent with previous studies, type I NBs of the central brain typically re-entered the cell cycle by 26hr ALH, and stopped dividing around 24 hrs after pupal formation (APF) (Figure 2A). Expression of htl^{ACT} in glia (glial FGF activation) did not affect NB cell cycle entry (26hr ALH, Figure 2B-E), or their cell size at this time point (26hr ALH, Figure S1 C-D, M). It however delayed NB cell cycle exit at the end of neurogenesis (24hr APF, Figure 2F-I) indicated by the presence of increased number of Miranda $(Mira)^{+}$ NBs.

A second determinant of NB proliferation is asymmetric cell division, which is maintained through the establishment of cortical polarity in dividing NBs ((Wodarz, 2005), Figure 2J). We found that the percentage of NBs with correct localisation of basal cell fate determinants Miranda ((Shen et al., 1997), Figure 2N-P,

Q), and its adaptor protein Inscutable ((Doe, 1996), Figure 2K-M, Q) was significantly reduced upon *htl*^{ACT} expression in the glia. Consequently, we observed a change in the NB/GMC ratio from 2.30 to 2.07, suggesting that disruption of asymmetric divisions may have led to the production of more size-symmetric, as well as larger, daughter cells (Figure S1A-B). In support of this, the average size of NBs was significantly larger in brains with glial *htl*^{ACT} expression; this size difference was first observed at 48hr ALH, and diminished by early pupal stages (Figure S1 C-P). NB size enlargement has been linked to increased cellular growth (Hovhanyan et al., 2014; Rust et al., 2018; Song and Lu, 2011), consistent with this, we detected an increase in nucleoli size at 96 ALH (Figure S1K-L, Q), however, the ratio of NB nucleolar/cellular volume, which reflects cellular growth rate, was not significantly altered upon glial *htl*^{ACT} expression compared to control NBs (Figure S1R).

Next, we examined whether glial FGF signalling affects the speed of the NB cell cycle, and thus the rate of neuron production. At late L3, upon glial FGF activation with both pan-glial and cortex glial drivers, we observed a reduced rate of EdU incorporation (a readout of DNA synthesis) and pH3 (a marker of mitosis). Conversely, Htl inhibition resulted in an increase in NB mitotic index, without significantly altering the rate of EdU incorporation, suggesting that glial Htl activation inhibits NB cell cycle progression (Figure 3A-K). These results were confirmed by live cell imaging at mid L3, where NBs were labelled with Dpn::GFP (Figure 3N-P). The average cell cycle length (Figure 3M) was substantially longer upon FGF activation (from 100 minutes to 250 minutes), and shortened upon FGF inhibition (from 100 minutes to 68 minutes). To decipher which phase of the cell cycle was affected, we utilised the LexA/LexAop system to express *htl*^{ACT} in glial cells, and the Gal4 system to overexpress Fly-Fucci in NBs, where cell cycle phases can be identified using combinations of two fluorescent fusion proteins ((Zielke et al., 2014), Figure 3Q). We found a significant increase in the number of cells in G2/M, and G1-S, and a reduction in cells in G1 (Figure 3R-T), suggesting that NBs are stalled in the G2/M and G1/S phases of the cell cycle. Finally, several cell cycle genes such as Dacapo (data not shown) were upregulated in the NB upon glial FGF activation. Together, our data suggests that glial FGF activation prevents NB cell cycle progression, asymmetric division and its ability to produce the correct number of neuronal progeny and hence CNS size.

Lipid droplets and Hedgehog mediate the effects of glial FGF signalling on NB proliferation

To understand how FGF activation mediates glia-induced NB cell cycle defects, we assessed candidate mediators in glial cells. Lipid droplets (LD), which store triglycerides and cholesterol, reside in glial cells, and have previously been shown to protect NB proliferation against the effects of oxidative stress (Bailey et al., 2015). To visualise LDs in glia, we expressed FGF using Repo-gal4 and measured LDs using confocal microscopy. In all equivalent sample planes, we observed a consistent increase in LDs (visualised with the lipid dye Bodipy $^{493/503}$) upon glial FGF activation and a decrease in LDs when FGF signaling is inhibited (Figure 4A-D, Figure S2A). To explore this further, we assessed transcript levels of several genes involved in lipid metabolism. (Figure 4E, F). Amongst genes that promote lipogenesis, *fatty acid synthase-1* (*fasn1*, which produces long-chain fatty acids in the cytoplasm) (Smith et al., 2003), and *lipid storage droplet-2* (*lsd2*, which prevents the mobilisation of TAG from LDs) (Teixeira et al., 2003), were significantly upregulated upon FGF activation. Lipogenesis genes such as *acc* (which catalyses the conversion of Acetyl-CoA into malonyl-CoA) (Barber et al., 2005), *lipin* (which dephosphorylates phosphatidic acid into diacylglycerol (Ugrankar et al., 2011), as well as the lipase *brummer* were not significantly altered. As some of the enzymes involved in key steps of neutral fat storage were upregulated upon FGF activation, we conclude that an increase in lipogenesis is induced by FGF upregulation in the glia.

To test whether lipid metabolism is required downstream of glial-FGF activation, we knocked down lipogenesis genes *fasn1*, *lsd2*, as well as *dgat1* (diacylglycerol O-acyltransferase) (knockdown efficiency verified by lipid droplet reduction in Figure S2B-E). While not required for wildtype NB proliferation (Figure S2L-M), downregulation of these genes significantly rescued NB proliferation caused by glial-FGF activation (Figure 4G, Figure S2F-G), without affecting glial membrane morphology (except for *fasn1*, Figure S2 G,H-K). Together these results indicate that genes involved in lipid droplet formation lie downstream of glial-FGF activation to mediate glia-NB crosstalk.

To identify potential signalling pathways that facilitates glia-NB communication, we examined secreted molecules that are lipid-modified and are known to act in a paracrine fashion. Hedgehog (Hh), a morphogen that plays an important role in tissue patterning, was previously reported to be associated with circulating lipoproteins (Rodenfels et al., 2014). In addition, Hh signalling has been shown to regulate larval NB cell cycle speed and asymmetric division (Chai et al., 2013). Strikingly, we found that Hh is closely associated with lipid droplets in the cortex glia, exhibiting a stereotypical ring-like distribution around LDs. LDs were visualised with either a neural lipid stain, lipidTOX or a Lsd2::GFP reporter; whereas Hh was visualised with either an antibody, or a BAC encoded Hh:GFP (Chen et al., 2017)(Figure 4 H-L''' and Figure S3). At mid-L3 to pupal stages, Hh puncta surrounding LDs were mostly found in cortex glial cells (Figure 4H-I''', L-L''', Figure S2N, Figure S3A-D'') but were largely absent in superficial glial cells (Figure 4L-L''', Figure S3 A-B'', Figure S2N) and at earlier stages of development in all glia (Figure S3I-J''). The strong association of LDs and Hh appears to be central brain specific, as LDs in the optic lobe (IPC, white arrows, Figure 4H,J-J'''), and the wing imaginal disc (FigureS3 E-H'''), did not exhibit this association. Upon FGF activation, we detected a significant increase in Hh at both transcript and protein level (~8 fold, Figure 5A-B', D-E); whereas, upon FGF inhibition, a significant decrease in Hh was detected at the protein level but not at the transcript level (Figure 5C-C', D-E).

To assess whether Hh mediates glia-NB crosstalk downstream of FGF-activation, we performed three experiments. Firstly, we overexpressed *hh* in glial cells, and found that the speed of the NB cell cycle was decreased, and the cell fate determinant Mira was mislocalised, closely phenocopying the impact of glial FGF activation (Figure 5F-G, L, 5M). Secondly, Hh knockdown caused a mild increase in the speed of the NB cell cycle (Figure S4 A-B), suggesting that Hh negatively regulates NB cell cycle progression. Thirdly, Hh depletion in glia where FGF was ectopically activated was sufficient to restore NB cell cycle speed (Figure 5 H-K, N), without changing glial or LD volume (Figure S4 C-F). Collectively, this suggests that Hh mediates glia-NB crosstalk downstream of glial FGF activation.

To assess the signaling cascade downstream of glial Hh signalling, we assayed for the genes altered in the NBs when FGF signalling is activated in glial cells with

RNAseq (data not shown). Amongst the most significantly upregulated genes, was the downstream Hh effector *ci*, suggesting that glial FGF activates NB Hh signalling. Next, we asked if activation of NB Hh signalling pathway affects its proliferation. Overexpression of an activated form of *ci* (ci^{ACT}), significantly reduced NB division rate (Figure 5O-P, U); phenocopying the effects of glial-specific FGF activation and *hh* overexpression. Finally, we asked if inhibition of NB Hh signalling is epistatic to glial FGF-activation. We achieved this with a binary expression system, where a glial LexA/LexAop was used in conjunction with a NB Gal4/UAS, to simultaneously activate glial FGF signalling while inhibiting NB Hh signalling (Figure 5V). NB specific-Ci knockdown significantly rescued the cell cycle defects induced by glial-FGF activation (Figure 5 Q-T, W-X), suggesting that NB Hh signalling lies downstream of glial-FGF activation.

Lsd2 regulates Hh localisation and activity

As our data indicated that lipid metabolism and Hh signalling both lie downstream of FGF signaling in glia, we sought to address whether there is crosstalk between these two pathways. Upon *hh* overexpression (Figure S5 A, B), or *hh* knockdown (in a glial-FGF activation setting, Figure S4, E-F), no significant change in LDs were detected (Figure S5 A', B'), suggesting that Hh lies downstream of lipid droplet formation. Consistent with this, overexpression or knockdown of Lsd2 is capable of altering Hh sub-cellularization localisation. In control brains, Hh is localized to a stereotypical ring-like structure, where it is closely associated with LDs, and upon Lsd2 knockdown or overexpression, their distribution became more cytoplasmic, indicating that Hh-LD association maybe lost (yellow arrows, Figure S5 C-F). Similar, upon glial-FGF activation, we observed a change in Hh localization, this is partially restored by Lsd2 knockdown in the glia (yellow arrows, Figure S5 G-J). Together, these results led us to speculate that Lsd2 might play a role in releasing Hh from LDs to enhance its intracellular trafficking and ability to activate Hh signalling in the NBs. In support of this, glial-knock down of Lsd2 suppressed the impact of both FGF-activation (Figure 4G) and *hh* overexpression (Figure S5 N-S) on NB proliferation. This suggests that Lsd2 is required to modulate Hedgehog activity in the glia, which in turn affects NB proliferation.

Palmitoylation is required for glial Hh signalling

Lipids can function directly as signal molecules, or indirectly by modifying proteins to affect their activity, range of action or subcellular localization (Nusse, 2003). Posttranslational modifications of Hh modulate its biological activity (Nusse, 2003) (Figure 6A). The N- and C-termini of Hh proteins are covalently modified with palmitate and cholesterol, respectively (Pepinsky et al., 1998; Porter et al., 1996). We first tested whether cholesterol modification is important for the FGF mediated glia-NB crosstalk. NPC1 (Dispatched) is required for the release of cholesterol-modified Hh from secreting cells (Burke et al., 1999), and NPC2 is responsible for redistribution of cholesterol to the endoplasmic reticulum (ER) (Infante et al., 2008; Sleat et al., 2004). Acyl coenzyme A (CoA)/cholesterol acyltransferase 1 (ACAT), converts cholesterol into cholesterol esters (Bujold et al., 2010). When we knocked down either Dispatched, Npc2b, or ACAT1 we did not detect significant alterations to the NB cell cycle in the context of glial FGF activation (Figure 6B), suggesting that cholesterol modification is not required for this process. Consistent with this, glial-overexpression of HhN (Gorfinkiel et al., 2005), a Hh molecule without the cholesterol moiety - was sufficient to induce NB cell cycle slow down (Figure 6C-E), and make contact with NBs (Figure 6F-F''), suggesting that the function of glial Hh is not dependent on cholesterol modification.

The N-terminal amino acid of the Hh protein is covalently attached to palmitate (either provided in the diet or synthesized by *de novo* lipogenesis) by the enzyme Hh acyltransferase (*rasp* in *Drosophila* (Figure 6A)). In the embryo, Rasp has been shown to be required for Hh diffusion (Chamoun et al., 2001; Lee and Treisman, 2001; Micchelli et al., 2002). We asked whether palmitoylation of Hh is required for signalling downstream of FGF signalling, by knocking down Rasp. Rasp knockdown via two independent RNAi lines significantly rescued the cell cycle speed slow down induced by glial FGF activation (Figure 6 G-K). Together, our data suggests that palmitoylation, rather than cholesterol modification, is required for Hh activity in the context of glia-NB crosstalk.

Glial ROS acts in parallel to lipid-Hh signaling to regulate NB proliferation

Accumulation of lipid droplets in glia has previously been linked to reactive oxygen species (ROS) (Bailey et al., 2015; Liu et al., 2015). Using a ROS-inducible gstD promoter-GFP reporter (Sykiotis and Bohmann, 2008), we detected a 5-fold increase in gstD-GFP upon FGF-activation in glia (Figure 7A-C). To determine the extent to which changes in ROS levels impact NB proliferation under glial FGF activation, we overexpressed a *UAS-catalase* transgene (Anderson et al., 2005) to suppress ROS. Reducing ROS in this context did not reduce glial membrane overgrowth (Figure 7D-E) or ameliorate lipid droplet accumulation (Figure 7F-G), but was effective in rescuing NB proliferation defects caused by glial FGF-activation (Figure 7H-J). Together, this data suggests that ROS and Hh-LD axes act in synergy to mediate the effects of glial-FGF activation on NB proliferation.

Discussion:

The glial niche has previously been shown to relay nutrient signals to NBs (Chell and Brand, 2010; Sousa-Nunes et al., 2011), and buffer NB proliferation against extrinsic stresses such as nutrient restriction and oxidative stress (Bailey et al., 2015; Cheng et al., 2011; Liu et al., 2015). In this study, we find signalling molecule Hh closely associate with intracellular organelles called lipid droplets, to regulate NB behavior during larval neurogenesis. Glial niche derived Hh ligand is normally maintained at low levels, to limit the activation of Hh signalling in the NB, in order to promote its cell cycle progression. Upon glial niche expansion via FGF-activation, accumulation of Hh, modulated by lipid metabolism, activates Hh-signalling in the NB, which in turn reduces NB proliferation, disrupts its asymmetric division, and cell cycle exit. Together with upregulation of oxidative stress, these two mediators limit the ability of NBs to produce its full repertoire of neurons and generate an appropriately sized nervous system when the glial niche is disrupted (summarized in Figure 7K).

In addition to the pool of Hh that was previously shown to be expressed in the GMCs and neurons (Chai et al., 2013), a major pool of Hh ligand that activate paracrine Hh signalling in the NBs reside in the glial niche. These ligands are tightly associated with LD, which in addition to its role as energy stores, have been shown to have roles in signalling (Welte, 2015). During neurogenesis, most of the Hh ligands

are bound to LDs, and the overall level of Hh is kept low, to prevent activation of Hh signalling in the NB. NB Hh-signalling has been shown to affect both the timing of NB cell exit and cell cycle progression via its interaction with temporal transcription factors (Chai et al., 2013). In addition, Hh pathway can also affect cycle regulators Dacapo, CycA, CycE and CycD through direct target gene activation (Biehs et al., 2010). Therefore, during normal development, in order to sustain NB proliferation, Hh levels and activity in the glia has to be limited.

So, how is Hh activity in the glia regulated? We find there are two main mechanisms, both centering on lipid metabolism. Firstly, Lsd2 and Hh interact on the surface of LDs in the glial niche, to limit Hh subcellular localisation and its ability to activate NB signalling. Secondly, *de novo* lipogenesis contributes to the generation of palmitate, which is important for Hh post-translational modification and its ability to signal. We further tested out our model by examining the effects of glial FGF hyperactivation on NB proliferation. Here, we observed a concurrent upregulation of Hh and LDs, disruption of Hh-LD association, resulting in changes in Hh localization, and consequent NB cell cycle slow-down. A second mediator of glia-NB crosstalk downstream of glial-FGF signalling appears to be ROS, which has previously been shown to be a potent inducer of glial lipid droplet accumulation during oxidative stress (Bailey et al., 2015; Liu et al., 2015; Marschallinger et al., 2020). However, ROS and lipid storage/Hh signalling appear to act in parallel downstream of glial FGF activation.

Together, we present a novel mechanism of glial niche-NB crosstalk during development, and in the context of glial overgrowth, which centers on Hh-LD interaction in the glia, that non-cell autonomously affect the ability of NBs to progress through the cell cycle, carry out asymmetric division, and exit the cell cycle.

Acknowledgements

We are grateful to Alex Gould, Thomas B. Kornberg, Isabelle Guerrero, Yu Cai, William Chia, Tatsushi Igaki, Joseph M. Bateman, Kieran Harvey, Helena Richardson, Gary Hime, Philip Batterham for generous sharing of antibodies and fly stocks. We would like to thank Bloomington Drosophila Stock Center, Vienna Drosophila Resource Center, Fly Stocks of National Institute of Genetics, KYOTO

Stock Center, Developmental Studies Hybridoma Bank and Addgene for fly stocks and plasmids. We would like to also thank OZDros for *Drosophila* quarantine, Peter MacCallum Cancer Institute Microscopy core and Biological Optical Microscopy platform at the University of Melbourne for technical assistance. We would like to thank Charles Robin, Mike Murray for sharing their microinjection facility with us. We are grateful to Sofya Golenkina, Kieran Harvey and Andrew Bailey for critical reading of the manuscript. Schematic pictures in the figures are created with BioRender. Q.D. is funded by a Melbourne Research Scholarship, L.Y.C is funded by an ARC Future Fellowship, L.Y.C's laboratory is supported by funding from the NHMRC, ARC and the Peter MacCallum Cancer Foundation.

Author contribution

Q.D, M.Z, F.F, T.L conducted the experiments; Q.D and L.Y.C designed the experiments and wrote the paper.

Declaration of Interests

The authors declare no competing interests.

Figure legends

Figure 1. FGF signalling regulates the volume of glial membrane surrounding NBs

Images in this and following figures are of central brains of late L3 stage, scale bar = 50 μm, unless otherwise specified. In all graphs, error bars showed standard error of the mean (Sleat et al.). Data information is described as: Mean ± SEM, n= the number of samples. (*) $p<0.05$ (**) $p< 0.01$, (***) $p< 0.001$, (****) $p < 0.0001$, (ns) $p>0.05$

A) Schematic showing central brain type I NBs (Reddy and Irvine) that undergo asymmetric division to self-renew and produce a GMC (pink), which terminally differentiate to generate two post-mitotic neurons (blue). Each NB is surrounded by its cortex glial niche chamber (in grey). FGF signalling regulates the glial niche surrounding NBs; constitutive activation of the FGF receptor *heartless* (htl^{ACT}) leads

to glial overgrowth (middle), and overexpression of a dominant negative form of *heartless* (htl^{DN}) impedes gliogenesis (right).

B-G) Representative images showing glial size in brains overexpressing htl^{ACT} or htl^{DN}. Surface glia (B-D, 0 □m depth), and cortex glia (E-G, 2-8□m depth) are visualised with repo-Gal4>GFP in grey. Pan-glial overexpression of htl^{ACT} increased the volume of surface (C) and cortex glia (F) in comparison to control brains (B, E) while htl^{DN} overexpression reduced the volume of surface glia (D) and cortex glia (G), compared to control (B, E). NBs are marked with yellow dashed lines.

H-J) Higher magnification images showing glia (repo-Gal4>GFP, in grey) and their associated NBs (Mira, red) in control and overexpression of htl^{ACT} or htl^{DN}.
The glial niche chambers are outlined with yellow dashed line in H, I.

K) Quantification of glial volumes represented as glial volume/ averaged NB number. Control (*w1118*): 3789 ± 248.80 μm^3, n = 14; htl^{ACT}: 24105 ± 868.70 μm^3 n=16; htl^{DN}: 2113 ± 58.34 μm^3, n=14.

Figure 2. Glial FGF signalling affects NB cell cycle exit and asymmetric division
A) Schematic showing post-embryonic neurogenesis, starting at 26 hrs ALH, and terminating at 24 hours APF, via terminal symmetric division. During neurogenesis, glial niche cells (grey) extend processes (48ALH) and form a chamber enclosing NBs (Reddy and Irvine) and their progeny (pink and blue).

B-E) Representative images showing that the timing of NB cell cycle entry (visualised by EdU incorporation, grey, 26ALH, region of interest is outlined in yellow) was not significantly altered by pan-glial (*repo-gal4>*) htl^{ACT} overexpression, quantified in (E), where EdU voxels were normalised to control. Control (*w1118*): 1 ± 0.08, n=19; htl^{ACT}: 0.96 ± 0.15, n=25.

F-I) Representative images showing that the number of CB NBs at 24hr APF (Mira, grey, yellow arrows, region of interest is outlined in yellow) was significantly

increased with pan-glial (*repo-gal4>*) htl^{ACT} overexpression compared to control, quantified in (I). Control (*w1118*): 21.25 ± 2.91, n = 8; htl^{ACT}: 35.75 ± 4.22, n = 8.

J) Schematic depicting NB asymmetric division. At the apical cortex, the Par complex (aPKC/Par3/Par6) is connected to the PINS/MUD/Gαi complex by the adaptor protein, Inscuteable (magenta). The apical complexes direct the localization of cell fate determinants (Brat/Pros/ Numb) and their adaptor proteins Mira (Reddy and Irvine) and PON to the basal cortex.

K-Q) Representative images showing mitotic NBs (pH3, blue) with normal (K, N) and aberrant (L, M, O, P) distributions of polarity proteins, Insc (K-M, magenta) and Mira (N-P, red). Insc is cytoplasmic, (L-M) and Mira is cytoplasmic and cortical (O-P) when htl^{ACT} is overexpressed (*np2222-gal4>* htl^{ACT}). NBs are outlined with yellow dashed lines. Scale bar = 10 μm.

Q) Quantification of aberrant localization in Control (*w1118*), Insc (8%, n = 50) and Mira (35.83%, n = 120), glial htl^{ACT} overexpression, Insc (27.45%, n=102) and Mira (53.06%, n = 147).

Figure 3. Glial FGF signalling regulates NB cell cycle speed

A-C, J) Representative images showing that pan-glial (*repo-Gal4*) htl^{ACT} overexpression and not htl^{DN} overexpression significantly reduced the rate of NB (Mira, red) EdU incorporation (grey), quantified in (J). Control (*w1118*): 1 ± 0.02, n= 15; htl^{ACT}: 0.78 ± 0.02, n = 14; htl^{DN}: 0.97 ± 0.02, n = 15. In A-C, NBs positive for EdU are outlined with yellow dashed lines.

D-F, K) Representative images showing that the percentage of NBs (Mira, red) in mitosis (pH3, Cyan) was significantly reduced by pan-glial (*repo-Gal4*) htl^{ACT} overexpression, and significantly increased by htl^{DN} overexpression (*repo-gal4 >*), quantified in (K). Control (*w1118*): 32.81% ± 1.06%, n = 20; htl^{ACT}: 28.48% ±1.47%, n = 12; htl^{DN}: 45.94% ± 1.80%, n = 10. In D-F, NBs positive for pH3 are outlined with yellow dashed lines.

G-I, L) Representative images showing that cortex glial (*np2222-gal4*) overexpression of htl^{ACT} and htl^{DN} was sufficient to alter the EdU incorporation (grey) of NBs (Mira, red), quantified in (L). Control (*w1118*): 1 ± 0.02, n= 10; htl^{ACT}: 0.78 ± 0.02, n = 16; htl^{DN}: 0.94 ± 0.02, n = 10. In G-I, NBs positive for EdU are outlined with yellow dashed lines.

N-P, M) Representative still images from live imaging at mid L3 (Histone RFP, grey; Dpn::GFP, red) showing NB cell cycle length (measured as the length between consecutive divisions) was significantly increased, by pan-glial (*repo-gal4*) htl^{ACT} overexpression, and significantly reduced by glial htl^{DN} overexpression, quantified in (M). Control (*w1118*): 100.2 ± 6.04 mins, n= 25; htl^{ACT}: 250.00 ± 28.40 mins, n = 6; htl^{DN}: 68.44 ± 3.57mins, n = 36. Scale bar = 10 μm. NBs are outlined with blue dashed lines.

Q) Schematic depicting concurrent glial FGF activation (*repo-lexA >lexAop-*htl^{ACT}), and NB overexpression of fly-FUCCI (*dnab-gal4>UAS-GFP::E2F1, UAS-RFP::CycB*). The fly-FUCCI system utilizes the fusion protein GFP::E2F1 (a marker for cells in G2, M and G1phase) and RFP::CycB (a marker for cells in S, G2, M phase) to monitor cell cycle progression. Cells in G1 phase are GFP^+ RFP^- (green), cells in G2 and M phase are GFP^+RFP^+ (yellow), and cells in S phase are GFP^-RFP^+ (Reddy and Irvine), whereas, cells in G1-S transition are weakly labelled by both GFP and RFP (grey).

R-T) Representative images showing that the percentage of NBs (Mira, grey, R and S) in G1 phase (GFP::E2F1, green, enclosed by green dashed lines) was significantly reduced, with significantly more cells stuck in G1-S transition (circled by grey dashed lines, S) and G2/M phase (GFP::E2F1, RFP::CycB, yellow, circled by yellow dashed lines), quantified in (T). Control (*w1118*): G1 (26.72% ± 2.79%, n = 9), G1-S transition (7.36% ± 1.18%, n = 9), S (1.99% ± 0.69%, n = 9), G2/M (63.93% ± 1.76%, n = 9); htl^{ACT}: G1(10.93% ± 1.02%, n = 10), G1-S transition (13.20% ± 1.43%, n = 10), S(3.08 % ± 0.38%, n = 10), G2/M(72.80% ± 1.76%, n = 10).

Figure 4. Glial-FGF activation affects NB proliferation via lipid droplet and Hh accumulation.

A-D) Representative images showing that the amount of lipid droplets in CBs (BODIPY, green, CB circled by yellow dashed line) was significantly increased by pan-glial (*repo-gal4*) htl^{ACT} overexpression, and significantly reduced by pan-glial htl^{DN} overexpression. (D) Quantification of lipid droplet areas at Z plane depth =1 from Figure S2 (A). Control (*w1118*): 6569 ± 508.80 μm^2, n= 14; htl^{ACT}: 13415 ± 1030 μm^2, n = 19; htl^{DN}: 3952 ± 248.40 μm^2, n = 16.

E) Schematic depicting lipogenesis and lipolysis. Lipogenesis begins with *de novo* synthesis of fatty acids by carboxylation of cytosolic acetyl-CoA via acetyl-CoA carboxylase (ACC) and elongation of fatty chain via fatty acid synthase (FASN, red). Dietary-derived and *de novo*-generated fatty acids are activated into fatty acylCoA, which re-localizes to ER and participates in triglyceride (TAG) synthesis with glycerol-3 phosphate (G3P). This process is mediated by a series of enzymes: glycerol-3-phosphate acyltransferase (GPAT), acylCoA acylglycerol-3-phasphte acyltransferases (AGPAT), Lipin (a phosphatidate phosphatase), diacylglycerol acyltransferase (DGAT, red). TAG is translocated from the ER to the core of the intracellular organelles called lipid droplets (Reddy and Irvine). On the surface of lipid droplets, a triglyceride lipase called Brummer (Bmm), and its inhibitor Lsd2 (Reddy and Irvine), antagonistically control TAG storage.

F) mRNA expression level (represented by log2 fold change relative to the control) of *fasn1* and *lsd2 was* significantly up regulated by pan-glial (*repo-gal4*) htl^{ACT} overexpression, compared to the control (*w1118*). *fasn1*: from 0 ± 0.10 to 0.80 ± 0.20, n = 3; *lsd2:* from 0 ± 0.26 to 1.32 ± 0.06, n = 3. Other lipogenesis genes *acc* and *lipin*, and lipolysis gene *bmm* transcripts were not significantly altered.

G) The slowdown of NB EdU incorporation due to cortex glial (*np2222-gal4*) overexpression of htl^{ACT}, was significantly rescued by overexpression of RNAis against *fasn1*, *dgat* and *lsd2* (red bars, 1.10 ± 0.02, n = 14; 1.10 ± 0.02, n =16; 1.15 ± 0.02, n = 8), compared to corresponding control RNAis (*mcherry Ri*, dark grey bars, 1.00 ± 0.02, n = 14; 1.10 ± 0.02, n =16, 1.10 ± 0.03, n = 14).

I-I''' are the enlarged view of H, magenta dashed square. J-J''' are enlarged view of H, yellow dashed square. L-L''', are enlarged view of K, magenta dashed square.

H- J''') Representative images showing at -6 μm relative to the surface, Hh (cyan) accumulates on the surface of lipid droplets (LipidTOX, red) in cortex glial cells (green) of the central brain (yellow arrows) but not of the inner proliferation center (IPC), white arrows.

K-L''') Representative images showing at -10 μm relative to the surface, lipid droplets and Hh are not closely associate in the glial cells located at the surface edge of the CB (white arrows), note their association in the cortex glial cells (yellow arrow).
Scale bar = 50 μm for H and K, Scale bar = 20 μm for I-I''', J-J''' and L-L'''.

Figure 5. The Hedgehog signalling pathway acts downstream of glial FGF signalling to regulate NB proliferation.
A-E) Representative images showing pan-glial (*repo-gal4 > GFP)* htl^{ACT} overexpression increased Hh levels, and pan-glial htl^{DN} overexpression significantly reduced Hh levels (antibody staining, cyan, outlined with yellow dashed line), quantified in (E). Control (*w1118*): 7.70 x10^5 ± 4.84 x 10^4 AU, n = 4; htl^{ACT}: 2.00 x 10^6 ± 1.90 x 10^5 AU, n = 6; htl^{DN}: 3.44 x 10^5 ± 4.59 x 10^4 AU, n = 6.

D) The relative mRNA level of *hh* (represented by log2 fold change relative to the control - *repo-gal4 > w1118*, n=3) was significantly up-regulated by *repo gal4 >* htl^{ACT} (n = 3, from 0 ± 0.40 to 3.17 ± 0.33), but not altered by *repo-gal4 >* htl^{DN} (n =3, from 0 ± 0.34 to 0.36 ± 0.04)

F-G, L-M) Representative images showing that pan-glial (*repo-gal4*) overexpression of *hh* was sufficient to reduce the number of EdU^+ NBs (Mira, red; EdU, grey), quantified in (L). Control (*w1118*): 1.00 ± 0.03, n = 16; *hh* overexpression: 0.86 ± 0.02, n = 20. EdU^+ NBs are circled with yellow dashed lines in F-G, H-K, O-T.

Pan-glial (*repo-gal4*) overexpression of *hh* increased mis-localization of Mira (images not shown), quantified in (M) (from 33.33%, n = 150 to 57.89%, n= 76). Control = *w1118.*

H-K, N) Representative images showing that cortex glial (*np2222-gal4*) overexpression of two independent RNAis against *hh* consistently and significantly rescued EdU incorporation defects caused by htl^{ACT} overexpression, quantified in (N). *Control Ri* (*mcherry Ri*): 1.00 ± 0.02, n = 7; $hhRi^{V43255}$: 1.12 ± 0.02, n = 12. *Control Ri* (*mcherry Ri*): 1.00 ± 0.03, n = 14 (same data set as 5th column in Figure 4G); $hhRi^{BL25794}$: 1.16 ± 0.03, n = 11.

O-P, U) Representative images showing that NB (*dnab-gal4*) overexpression of a constitutively activated form of *ci* (ci^{ACT}) reduced NB EdU index, quantified in (U). Control (*w1118*): 1.00 ± 0.02, n = 12; ci^{ACT} overexpression: 0.85 ± 0.02, n = 10.

Q-X) Schematic V depicts Gal4-UAS and LexA-LexAop dual expression system used for Q-T and W-X. *repo-LexA>LexAop* htl^{ACT} reduced NB proliferation as indicated by EdU incorporation, quantified in (W). Control (*w1118*): 1.23 ± 0.02, n = 10; htl^{ACT}: 1.00 ± 0.04, n = 10 (data normalised to htl^{ACT}).
Knocking down NB hedgehog signalling (*dnab-gal4 > UAS-ciRNAi*) significantly rescued NB cell cycle slow down induced by glial htl^{ACT} overexpression (*repo-lexA > LexAop* htl^{ACT}), quantified in (X). *Control Ri* (*GFP Ri*): 1.00 ± 0.03, n = 30; *ci* $Ri^{HMJ23860}$: 1.15 ± 0.02, n = 26; *Control Ri* (*GFP Ri*): 1.00 ± 0.02, n = 12; *ci* $Ri^{NIG2125R2}$: 1.17 ± 0.03, n = 7.

Figure 6. Glia-NB crosstalk is mediated by palmitoylated Hh

A) Schematic depicting Hh auto-processing in the endoplasmic reticulum, which starts with the cleavage of the protein into a C-terminal part (Hh-C, yellow) and a N-terminal part (Hh-N, blue), with simultaneous covalent addition of cholesterol. Palmitate, from either diet or *de novo* lipogenesis (via ACC and FASN), is added onto Hh-N, in a reaction catalysed by an acyltransferase, encoded by *rasp*.

B) Inhibition of cholesterol trafficking (by *dispatched RNAis* and *npc2b RNAi*) or cholesterol esterification (by *ACAT RNAi*) did not significantly alter NB cell cycle speed slow down induced by cortex glial *(np2222-gal4)* htl^{ACT} overexpression (images not shown). *Control Ri* (*mcherry Ri*): 1.00 ± 0.02, n = 12; *disp* $Ri^{BL27247}$: 0.97 ± 0.02, n = 12. *Control Ri* (*mcherry Ri*): 1.00 ± 0.03, n = 14; *disp* Ri^{V10004}: 1.00 ± 0.03, n = 10. *Control Ri* (*mcherry Ri*): 1.00 ± 0.02, n = 12 (same as the 1st column); *npc2b Ri*: 1.02 ± 0.04, n = 9. *Control Ri* (*mcherry Ri*): 1.00 ± 0.02, n = 11; *ACAT Ri*: 1.07 ± 0.03, n = 13.

C-E) Representative images showing that ectopic overexpression of Hh.N.EGFP in cortex glia (*np2222*-gal4) reduced the rate of NB EdU incorporation, compared to control (*w1118*), quantified in (E). Control (*w1118*): 1.00 ± 0.01, n = 13; *hh.N.EGFP* overexpression: 0.75 ± 0.03, n = 12. Edu+ NBs (Mira, red; EdU, grey) are circled with yellow dashed line.

F-F'') Representative images showing that a EGFP tagged Hh-N fragment, lacking the cholesterol moiety (Hh.N.EGFP, cyan), when ectopically overexpressed in cortex glia (*np2222-gal4*), was associated with NBs (Mira, red, yellow arrow heads indicate Hh.N-NB contact). Scale bar = 20 μm.

G-K) Representative images showing that the inhibition of palmitoylation (via two independent rasp *RNAis*) rescued NB cell cycle slowdown induced by cortex glial *(np2222-gal4)* htl^{ACT} overexpression, quantified in (K). *Control Ri* (*mcherry Ri*): 1.00 ± 0.02, n = 18; *rasp* $Ri^{NIG11495R1}$: 1.10 ± 0.02, n = 21. *Control Ri* (*mcherry Ri*): 1.00 ± 0.02, n = 26; *rasp* $Ri^{NIG11495R2}$: 1.07 ± 0.02, n = 29. Edu+ NBs (Mira, red; EdU grey) are circled with yellow dashed line.

Figure 7 Glial ROS mediates glial-FGF dependent NB cell cycle regulation, independently of lipid droplets and Hh.

A-C) Representative images showing that oxidative stress (gstD-GFP, green) was significantly increased, by cortex glial (*np2222-gal4*) overexpression of htl^{ACT},

quantified in (C) (region of interest outlined with yellow dashed lines). Control (*w1118*): 2.42 x 10^7 ± 8.51 x 10^5, n = 4; htl^{ACT}: 1.31 x 10^8 ± 4.56 x 10^6, n = 3.

D-J) Representative images showing that overexpression of *Cat.A*, an inhibitor of ROS, in cortex glia (*np2222-gal4>GFP*), significantly rescued NB EdU incorporation caused by htl^{ACT} overexpression (*Control: UAS-lacZ*: 1.00 ± 0.02, n = 12; *Cat.A* overexpression: 1.08 ± 0.02, n = 12), but did not significantly altered glial volume or the amount of lipid droplets (region of interest outlined with yellow dashed line, LipidTOX, red). EdU+ NBs (Mira, red; EdU, grey) are circled with yellow dashed line in H-I.

K) A model depicting the regulatory network underlying glial FGF and NB crosstalk. In 3rd instar central brain, NBs reside in a microenvironment, composed of glial cells, where Hh (blue) is associated with lipid droplets (left panel). Activation of the FGF signalling pathway in the glial niche leads to a dramatic glial overgrowth and an increase in the expression of Hh as well as lipid droplet storage, which is caused by upregulation of two lipid droplet storage promoting enzymes-FASN1 and Lsd-2. Upregulation of FASN1 promotes *de novo* lipogenesis, which contributes to the generation of palmitate, required for Hh palmitoylation in the ER (1, greybox). Upregulation of Lsd2, an inhibitor of lipolysis on the surface of lipid droplet, releases Hh from lipid droplets and facilitates its intracellular trafficking (2, greybox). After processing in the ER and lipid droplets, Hh is secreted from glia to activate the Hedgehog signalling pathway of NBs and consequently, slows down their proliferation (pink box). In addition, ROS is also upregulated upon glial FGF activation and acts in parallel to the lipid metabolism-Hh axis to regulate NB proliferation via an unknown mechanism (dashed line, grey box). In the grey box, all the lipid metabolism and lipid modification steps are highlighted in red, the Hh processing routes are highlighted in blue.

Tables

Table 1 (related to **Method and Materials**)

Target gene	Forward primer	Reverse primer	Source
rpl32	CCGCTTCAAGGGACAGTA TCTG	ATCTCGCCGCAGTAAACGC	(Akkouche et al., 2017)
fasn1	TAAGGAGGTCTGCACAAAGCC	CGGTGAGAGGGTGATGATCG	PrimerBlast
acc	CCTCATTAACCCGCGCTACA	TTTTCAGCGCAATGGTGGTC	PrimerBlast
lipin	AAACGAAGCTGAGACGGAGAA	GGTTTTGCTCTTGGACACCTC	FlyPrimerBank
lsd2	ATTGCCCGTGGTAAATGCG	CGAAGACACGATTTTTGCCTTT	FlyPrimerBank
bmm	GTCTCCTCTGCGATTTGCCAT	CTGAAGGGACCCAGGGAGTA	FlyPrimerBank
hh	TGCTCCGTCAAGTCAGATTCG	GTTGGCGGTCATGCTCAAAA	PrimerBlast

Method and materials

Fly husbandry and strains

Fly stocks were reared on standard *Drosophila* media at 25 °C. Crosses for overexpression and knockdown experiment were set up at 25 °C, and after a day, the progeny were moved to 29 °C, unless otherwise stated.

The fly strains used were: *repo-gal4* (BDSC7415), *np2222-gal4* (KYOTO112830), *dnab*-gal4 (From Alex Gould lab), *repo-lexA::GAD* (BDSC67096), w^{1118},*UAS*-

htl^{ACT}(BDSC5367), *lexAop-htl*^{ACT} (this paper), *UAS-htl*^{DN} (BDSC5366), *UAS-GFP*, *UAS-FUCCI* (BDSC55110), *UAS-lacZ*, *UAS-luc* (BDSC64774), *UAS-hh* (from Thomas B. Kornberg lab), *UAS-hh.N.EGFP* (BDSC81023), *UAS-lsd2* (from Alex Gould lab), *UAS-ci*$^{Nc5m5m(ACT)}$ (from Yu Cai lab), *UAS-cat.A* (BDSC24621), *UAS-mcherryRNAi* (BDSC35785), *UAS-GFPRNAi* (BSDC9331), *UAS-fasn1RNAis* (NIG3523R-2, NIG3523R-6), *UAS-lsd2RNAis* (VDRC102269, BDSC34617 and BDSC32846), *UAS-dgat1RNAi* (VDRC100003), *UAS-hhRNAis* (VDRC43255, BDSC25794), *UAS-ciRNAis* (NIGHMJ23860, NIG2125R-2), *UAS-dispRNAis* (VDRC10004, BDSC27247), *UAS-npc2bRNAi* (BDSC), *UAS-raspRNAis* (NIG11495R-1, NIG11495R-2), *UAS-ACATRNAi* (BDSC63035), *dpnGFP* (BDSC59755), *his2AV-mRFP* (Kieran Harvey lab), *hh(BAC)GFP* (from Thomas B. Kornberg lab), *lsd2YFP* (KYOTO115301), *gstD-GFP* (From Tatsushi Igaki lab). The *repo*-MARCM stock was: *UAS-RedStinger; repo-flp, repo-gal4, UAS-actinGFP; FRT82B, tub-gal80* (from Joseph M. Bateman lab). *w;;FRT82B* was used to generate surface glial clones.

Immunostaining, EdU and Lipid droplet staining

Larval and pupal brains were dissected out in PBS, fixed for 25 minutes in 4% formaldehyde in PBS and rinsed in 0.5% PBST (PBS + 0.5% TritonX-100). For immunostaining, brains were incubated with primary antibodies overnight at 4 °C, followed by an overnight secondary antibody incubation at 4 °C. Samples were mounted in 80% glycerol in PBS for image acquisition. The primary antibodies used were mouse anti-Mira (1:50; gift of Alex Gould), rat anti-Mira (1:100, Abcam), rat anti-pH3 (1:500; Abcam), chick anti-GFP (1:2000; Abcam), rabbit anti-RFP (1:100, Abcam), mouse anti-Fibrillarin (1:200, Abcam), rabbit anti-Hh (1:500, gift of Isabel Guerrero), rabbit anti-Insc (1:20,gift from William Chia). Secondary donkey antibodies conjugated to Alexa 555 and Alexa 647 and goat antibody conjugated to Alexa 488, 555 and 647 (Molecular Probes) were used at 1:500.

For EdU incorporation experiment, late 3rd instar larval brains were incubated together in 10 μM EdU /PBS for 15 mins before fixation. EdU incorporation was detected with a Click-iT Plus EdU Cell Proliferation Kit for imaging, Alexa Fluor 647 dye (Invitrogen), following the manufacturer's instruction. The brain tissues were

then stained with the neuroblast marker, Mira. In the procedure, control brains and experimental brains were processed in the same tube. 26ALH larval brains were dissected and incubated in EdU for 1hr before fixation.

For lipid droplet staining, late 3rd instar larval brains were dissected out in PBS, fixed, and rinsed three times in PBS. The tissues were then incubated in either BODIPY 493/503 (Invitrogen, 1:500 in PBS) or HCS LipidTOX Red Neutral Lipid Stain (Invitrogen, 1:1000 in PBS) for 1 hour, and then rinsed three times in PBS. To keep the morphology of lipid droplets, the brain tissues were mounted in PBS and imaged immediately. For experiments that require lipid droplet staining together with immune-staining, the tissues were rinsed three times in PBS after immunostaining to remove all PBST, and incubated with lipid droplet dyes as described above. The tissues were mounted in 80% glycerol in PBS for imaging. Images were collected on a Leica SP5 confocal microscope.

Live imaging

Dissected brains (72ALH) were cultured in Schneider's culture medium supplemented with 10% inactivated FBS, 2% Penicillin-Streptomycin solution, 20μM glutamine and Schneider's culture medium and dissected fat body from the same animals. The brains dissected out were imaged in a μ-Slide 8 well (Ibidi) on Olympus FV3000 microscope using resonance scanner in 16Bit mode, 40x/0.95 lens and 2x additional zoom-in. Z stacks with 2 μm intervals were captured every 2 minutes. Laser intensity was kept low to avoid cytotoxicity.

Quantitative reverse transcription PCR

For gene expression analysis, 20 dissected late 3rd instar larval brains were lysed in 300 μl TRI Reagent (ZYMO Research R2061) to form one biological replicate. Three biological replicates were prepared for each genotype: *repo gal4> w1118*, *repo gal4> htl^{ACT}* and *repo gal4> htl^{DN}*. Total RNA was extracted using a Direct-zol RNA Microprep Kit (ZYMO Research R2061) and 1μg of total RNA from each sample was reverse transcribed into cDNA using ProtoScript II First Strand cDNA Synthesis Kit (NEB, E6560S) according to the manufacturer's instructions. The qPCR was performed using the stepOnePlus real-time PCR system (Applied Biosystems) using

Fast SYBR Green master mix reagent (Applied Biosystems, 4385612). Gene expression levels were normalized to rpl32, and calculated using the $2^{-\Delta Ct}$ method. The primers were either designed using Primer-BLAST (https://www.ncbi.nlm.nih.gov/tools/primer-blast/), or obtained from FlyPrimerBank (https://www.flyrnai.org/flyprimerbank).

listed in Table 1.

Molecular cloning

A constitutively active form of *htl*, comprising the dimerization domain of the bacteriophage λ repressor, (described in (Michelson et al., 1998)) was amplified from the genomic DNA of the fly stock: *UAS-htl*^{ACT}(BDSC5367), using a forward primer, 5'-CAACTGCAACTACTGAAATCTGCC-3', and a reverse primer 5'-CCCCCTCTAGATTAATAATTACACCACTTCTGC. The resulting PCR product was digested with *Not*I (Promega, Cat#R6431) and *Xba*I (Promega, Cat#R6181), which cut at the restriction site as indicated by underlining in the reverse primer above. The plasmid, *pJFRC19-13XLexAop2-IVS-myr::GFP* (Addgene_26224), was identically digested to remove *myr::GFP*. The restriction fragment, *Not*I-htl^{ACT}-*Xba*I, was subsequently cloned into the digested lexAop vector (Pfeiffer et al., 2010). The reconstructed plasmid was sequenced and injected into flies carrying an attP2 docking site (BL25710). The overexpression of *lexAop-htl*^{ACT} using *repo-lexA* recapitulates the glial overgrowth caused by *UAS-htl*^{ACT} overexpression using *repo-gal4* (data not shown).

Volume and size measurement

Total volume of glial nucleus plus membrane (*repo-gal4>UAS-GFP*) were measured from three-dimensional reconstruction of 2-μm spaced confocal Z stacks with Volocity software (Improvision). The glial volume was further normalized to central brain NB number of each brain lobe, to quantify glia surrounding each NB. Neuroblast (Mira^{+} or Dpn^{+}) and nucleoli (Fib^{+}) diameter was estimated by averaging orthogonal measurements of diameter, with a single confocal section on Fiji (https://imagej.net/Fiji). Nucleolar and nuclear volumes were calculated with the formula $4/3\pi r^3$. Nucleoli/Nucleus ratio = nucleolar volume/ nuclear volume.

Cell cycle speed measurement

For 26ALH larval brains, EdU+ voxels of the whole brain were measured with Volocity software (Improvision) to indicate neuroblast re-entry into cell cycle. Normalized EdU voxels were calculated by normalizing the EdU voxels to the mean voxel counts of the control. For late L3 larval brains, the number of EdU^+ Type I NBs ($Mira^+$; distinguished from Type II NBs by morphological features) was counted in the central brain of each brain lobe. EdU index was determined by normalizing the number of EdU^+ Type I NBs to the average number of EdU^+ Type I NBs in the control. The pH3 index was calculated as the percentage of Type I NBs in M phase ($pH3^+$).

Lipid droplet area measurement

For brain samples with BODIPY staining, Z stacks with 2 μm intervals were captured from the surface to the deeper section where lipid droplets are no longer detected (Control: -32 μm; htl^{ACT}: -56-64 μm; htl^{DN}: -32 μm), and were categorized into 8 Z depth positions relative to the surface. We quantified BODIPY signal area for each Z stack images, on Fiji using auto-threshold function (Moments, (Tsai, 1985)) by the following procedure: Draw ROI around each brain lobe (freehand selections) > duplicate hyperstack>Edit> Clear outside> Adjust> Threshold> Moment method > Auto and apply> Analyse particles> area data of each Z stack image was generated. The BODIPY signal area of each Z depth position was determined by averaging BODIPY area of images within each Z depth position. BODIPY signal area was plotted against the z depth position relative to the surface (0-7) in S2A, and the BODIPY area of 'z depth 1", where lipid droplets accumulated, was plotted in Figure 4C.

Protein total intensity (Figure 5 and 7)

The single confocal image was used for the intensity measurement on Fiji using the formula: CTCF (corrected total cell fluorescence) = Integrated density – (Area of selected cell x mean fluorescence of background readings) (McCloy et al., 2014).

Statistical analysis

P-values are calculated by two-tailed, unpaired Student's *t*-test, with equal sample variance; The Welch's correction was applied in case of unequal variances. Mann-Whitney test was used when data deviated from a normal distribution. For all histograms, error bars represent SEM.

REFERENCES

Akkouche, A., Mugat, B., Barckmann, B., Varela-Chavez, C., Li, B., Raffel, R., Pelisson, A., and Chambeyron, S. (2017). Piwi Is Required during Drosophila Embryogenesis to License Dual-Strand piRNA Clusters for Transposon Repression in Adult Ovaries. Mol Cell *66*, 411-419 e414.

Anderson, P.R., Kirby, K., Hilliker, A.J., and Phillips, J.P. (2005). RNAi-mediated suppression of the mitochondrial iron chaperone, frataxin, in Drosophila. Hum Mol Genet *14*, 3397-3405.

Avet-Rochex, A., Kaul, A.K., Gatt, A.P., McNeill, H., and Bateman, J.M. (2012). Concerted control of gliogenesis by InR/TOR and FGF signalling in the Drosophila post-embryonic brain. Development *139*, 2763-2772.

Bailey, A.P., Koster, G., Guillermier, C., Hirst, E.M., MacRae, J.I., Lechene, C.P., Postle, A.D., and Gould, A.P. (2015). Antioxidant Role for Lipid Droplets in a Stem Cell Niche of Drosophila. Cell *163*, 340-353.

Barber, M.C., Price, N.T., and Travers, M.T. (2005). Structure and regulation of acetyl-CoA carboxylase genes of metazoa. Biochim Biophys Acta *1733*, 1-28.

Biehs, B., Kechris, K., Liu, S., and Kornberg, T.B. (2010). Hedgehog targets in the Drosophila embryo and the mechanisms that generate tissue-specific outputs of Hedgehog signaling. Development *137*, 3887-3898.

Bjornsson, C.S., Apostolopoulou, M., Tian, Y., and Temple, S. (2015). It takes a village: constructing the neurogenic niche. Dev Cell *32*, 435-446.

Bujold, M., Gopalakrishnan, A., Nally, E., and King-Jones, K. (2010). Nuclear receptor DHR96 acts as a sentinel for low cholesterol concentrations in Drosophila melanogaster. Mol Cell Biol *30*, 793-805.

Burke, R., Nellen, D., Bellotto, M., Hafen, E., Senti, K.A., Dickson, B.J., and Basler, K. (1999). Dispatched, a novel sterol-sensing domain protein dedicated to the release of cholesterol-modified hedgehog from signaling cells. Cell *99*, 803-815.

Chai, P.C., Liu, Z., Chia, W., and Cai, Y. (2013). Hedgehog signaling acts with the temporal cascade to promote neuroblast cell cycle exit. PLoS Biol *11*, e1001494.

Chamoun, Z., Mann, R.K., Nellen, D., von Kessler, D.P., Bellotto, M., Beachy, P.A., and Basler, K. (2001). Skinny hedgehog, an acyltransferase required for palmitoylation and activity of the hedgehog signal. Science *293*, 2080-2084.

Chell, J.M., and Brand, A.H. (2010). Nutrition-responsive glia control exit of neural stem cells from quiescence. Cell *143*, 1161-1173.

Chen, W., Huang, H., Hatori, R., and Kornberg, T.B. (2017). Essential basal cytonemes take up Hedgehog in the Drosophila wing imaginal disc. Development *144*, 3134-3144.

Cheng, L.Y., Bailey, A.P., Leevers, S.J., Ragan, T.J., Driscoll, P.C., and Gould, A.P. (2011). Anaplastic lymphoma kinase spares organ growth during nutrient restriction in Drosophila. Cell *146*, 435-447.

Ding, R., Weynans, K., Bossing, T., Barros, C.S., and Berger, C. (2016). The Hippo signalling pathway maintains quiescence in Drosophila neural stem cells. Nat Commun *7*, 10510.

Doe, C.Q. (1996). Spindle orientation and asymmetric localization in Drosophila: both inscuteable? Cell *86*, 695-697.

Doe, C.Q. (2017). Temporal Patterning in the Drosophila CNS. Annu Rev Cell Dev Biol *33*, 219-240.

Gorfinkiel, N., Sierra, J., Callejo, A., Ibanez, C., and Guerrero, I. (2005). The Drosophila ortholog of the human Wnt inhibitor factor Shifted controls the diffusion of lipid-modified Hedgehog. Dev Cell *8*, 241-253.

Homem, C.C., and Knoblich, J.A. (2012). Drosophila neuroblasts: a model for stem cell biology. Development *139*, 4297-4310.

Hovhanyan, A., Herter, E.K., Pfannstiel, J., Gallant, P., and Raabe, T. (2014). Drosophila mbm is a nucleolar myc and casein kinase 2 target required for ribosome biogenesis and cell growth of central brain neuroblasts. Mol Cell Biol *34*, 1878-1891.

Infante, R.E., Wang, M.L., Radhakrishnan, A., Kwon, H.J., Brown, M.S., and Goldstein, J.L. (2008). NPC2 facilitates bidirectional transfer of cholesterol between

NPC1 and lipid bilayers, a step in cholesterol egress from lysosomes. Proc Natl Acad Sci U S A *105*, 15287-15292.

Isshiki, T., Pearson, B., Holbrook, S., and Doe, C.Q. (2001). Drosophila neuroblasts sequentially express transcription factors which specify the temporal identity of their neuronal progeny. Cell *106*, 511-521.

Lee, J.D., and Treisman, J.E. (2001). Sightless has homology to transmembrane acyltransferases and is required to generate active Hedgehog protein. Curr Biol *11*, 1147-1152.

Liu, L., Zhang, K., Sandoval, H., Yamamoto, S., Jaiswal, M., Sanz, E., Li, Z., Hui, J., Graham, B.H., Quintana, A., et al. (2015). Glial lipid droplets and ROS induced by mitochondrial defects promote neurodegeneration. Cell *160*, 177-190.

Marschallinger, J., Iram, T., Zardeneta, M., Lee, S.E., Lehallier, B., Haney, M.S., Pluvinage, J.V., Mathur, V., Hahn, O., Morgens, D.W., et al. (2020). Lipid-droplet-accumulating microglia represent a dysfunctional and proinflammatory state in the aging brain. Nat Neurosci *23*, 194-208.

Maurange, C., Cheng, L., and Gould, A.P. (2008). Temporal transcription factors and their targets schedule the end of neural proliferation in Drosophila. Cell *133*, 891-902.

McCloy, R.A., Rogers, S., Caldon, C.E., Lorca, T., Castro, A., and Burgess, A. (2014). Partial inhibition of Cdk1 in G 2 phase overrides the SAC and decouples mitotic events. Cell Cycle *13*, 1400-1412.

Micchelli, C.A., The, I., Selva, E., Mogila, V., and Perrimon, N. (2002). Rasp, a putative transmembrane acyltransferase, is required for Hedgehog signaling. Development *129*, 843-851.

Michelson, A.M., Gisselbrecht, S., Buff, E., and Skeath, J.B. (1998). Heartbroken is a specific downstream mediator of FGF receptor signalling in Drosophila. Development *125*, 4379-4389.

Nusse, R. (2003). Wnts and Hedgehogs: lipid-modified proteins and similarities in signaling mechanisms at the cell surface. Development *130*, 5297-5305.

Pepinsky, R.B., Zeng, C., Wen, D., Rayhorn, P., Baker, D.P., Williams, K.P., Bixler, S.A., Ambrose, C.M., Garber, E.A., Miatkowski, K., et al. (1998). Identification of a palmitic acid-modified form of human Sonic hedgehog. J Biol Chem *273*, 14037-14045.

Pfeiffer, B.D., Ngo, T.T., Hibbard, K.L., Murphy, C., Jenett, A., Truman, J.W., and Rubin, G.M. (2010). Refinement of tools for targeted gene expression in Drosophila. Genetics *186*, 735-755.

Poon, C.L., Mitchell, K.A., Kondo, S., Cheng, L.Y., and Harvey, K.F. (2016). The Hippo Pathway Regulates Neuroblasts and Brain Size in Drosophila melanogaster. Curr Biol *26*, 1034-1042.

Porter, J.A., Young, K.E., and Beachy, P.A. (1996). Cholesterol modification of hedgehog signaling proteins in animal development. Science *274*, 255-259.

Read, R.D., Cavenee, W.K., Furnari, F.B., and Thomas, J.B. (2009). A drosophila model for EGFR-Ras and PI3K-dependent human glioma. PLoS Genet *5*, e1000374.

Reddy, B.V., and Irvine, K.D. (2011). Regulation of Drosophila glial cell proliferation by Merlin-Hippo signaling. Development *138*, 5201-5212.

Rodenfels, J., Lavrynenko, O., Ayciriex, S., Sampaio, J.L., Carvalho, M., Shevchenko, A., and Eaton, S. (2014). Production of systemically circulating Hedgehog by the intestine couples nutrition to growth and development. Genes Dev *28*, 2636-2651.

Rust, K., Tiwari, M.D., Mishra, V.K., Grawe, F., and Wodarz, A. (2018). Myc and the Tip60 chromatin remodeling complex control neuroblast maintenance and polarity in Drosophila. EMBO J *37*.

Shen, C.P., Jan, L.Y., and Jan, Y.N. (1997). Miranda is required for the asymmetric localization of Prospero during mitosis in Drosophila. Cell *90*, 449-458.

Sleat, D.E., Wiseman, J.A., El-Banna, M., Price, S.M., Verot, L., Shen, M.M., Tint, G.S., Vanier, M.T., Walkley, S.U., and Lobel, P. (2004). Genetic evidence for nonredundant functional cooperativity between NPC1 and NPC2 in lipid transport. Proc Natl Acad Sci U S A *101*, 5886-5891.

Smith, S., Witkowski, A., and Joshi, A.K. (2003). Structural and functional organization of the animal fatty acid synthase. Prog Lipid Res *42*, 289-317.

Song, Y., and Lu, B. (2011). Regulation of cell growth by Notch signaling and its differential requirement in normal vs. tumor-forming stem cells in Drosophila. Genes Dev *25*, 2644-2658.

Sousa-Nunes, R., Yee, L.L., and Gould, A.P. (2011). Fat cells reactivate quiescent neuroblasts via TOR and glial insulin relays in Drosophila. Nature *471*, 508-512.

Speder, P., and Brand, A.H. (2018). Systemic and local cues drive neural stem cell niche remodelling during neurogenesis in Drosophila. Elife *7*.

Sykiotis, G.P., and Bohmann, D. (2008). Keap1/Nrf2 signaling regulates oxidative stress tolerance and lifespan in Drosophila. Dev Cell *14*, 76-85.

Teixeira, L., Rabouille, C., Rorth, P., Ephrussi, A., and Vanzo, N.F. (2003). Drosophila Perilipin/ADRP homologue Lsd2 regulates lipid metabolism. Mech Dev *120*, 1071-1081.

Tsai, W.-H. (1985). Moment-preserving thresolding: A new approach. Computer Vision, Graphics, and Image Processing *29*, 377-393.

Ugrankar, R., Liu, Y., Provaznik, J., Schmitt, S., and Lehmann, M. (2011). Lipin is a central regulator of adipose tissue development and function in Drosophila melanogaster. Mol Cell Biol *31*, 1646-1656.

Welte, M.A. (2015). Expanding roles for lipid droplets. Curr Biol *25*, R470-481.

Witte, H.T., Jeibmann, A., Klambt, C., and Paulus, W. (2009). Modeling glioma growth and invasion in Drosophila melanogaster. Neoplasia *11*, 882-888.

Wodarz, A. (2005). Molecular control of cell polarity and asymmetric cell division in Drosophila neuroblasts. Curr Opin Cell Biol *17*, 475-481.

Zielke, N., Korzelius, J., van Straaten, M., Bender, K., Schuhknecht, G.F.P., Dutta, D., Xiang, J., and Edgar, B.A. (2014). Fly-FUCCI: A versatile tool for studying cell proliferation in complex tissues. Cell Rep *7*, 588-598.

Figure 1

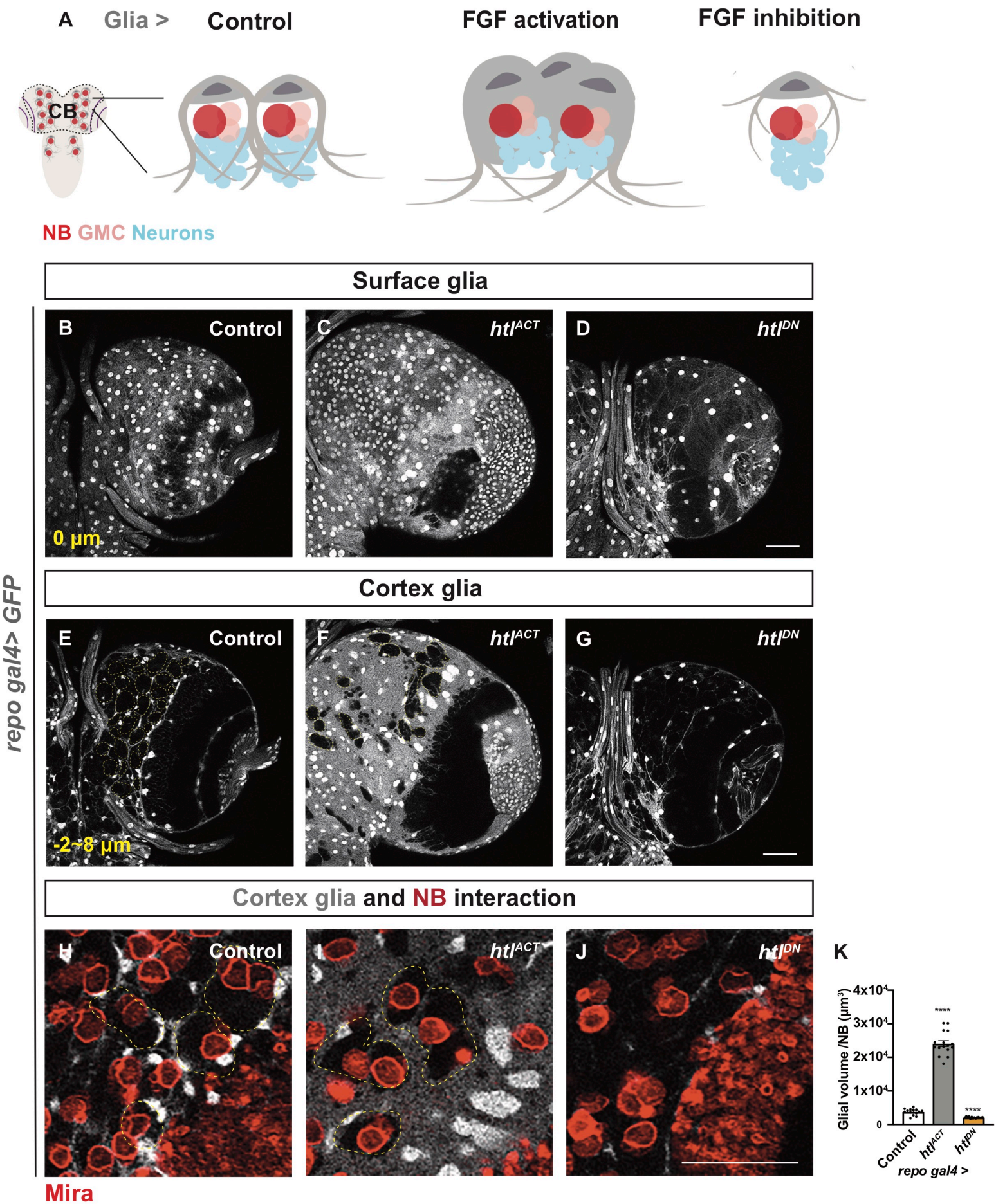

Figure 2

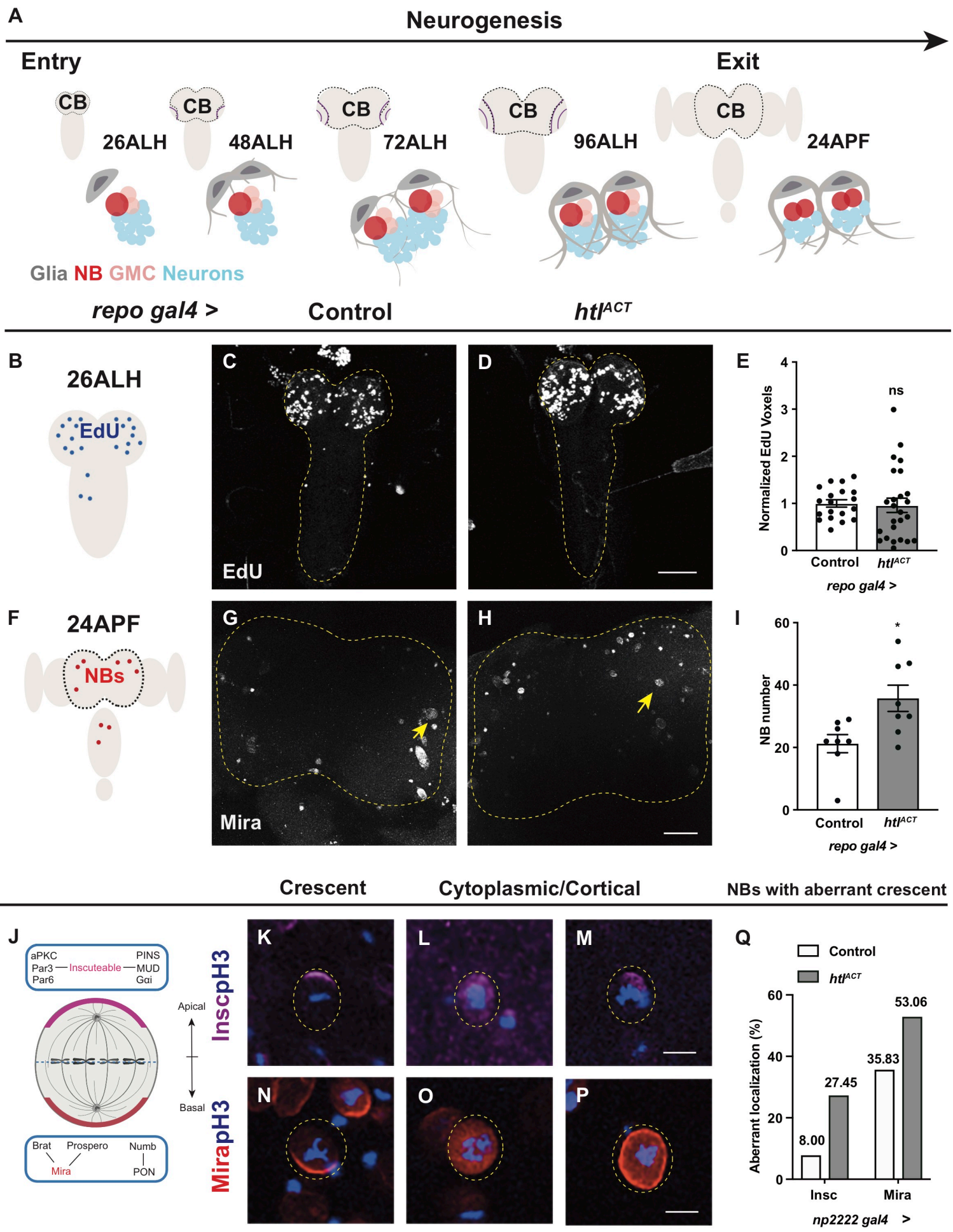

Figure 3

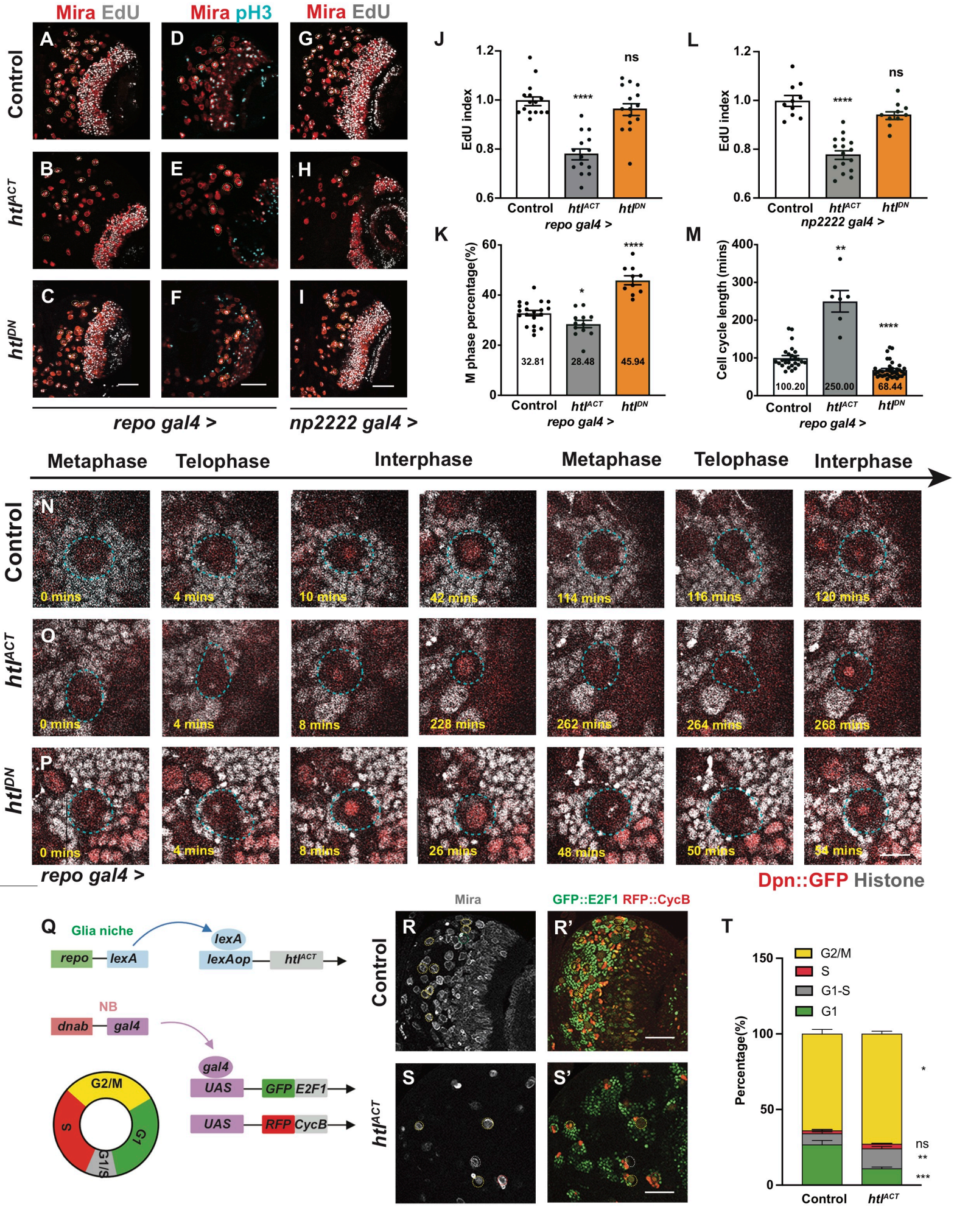

Figure 4

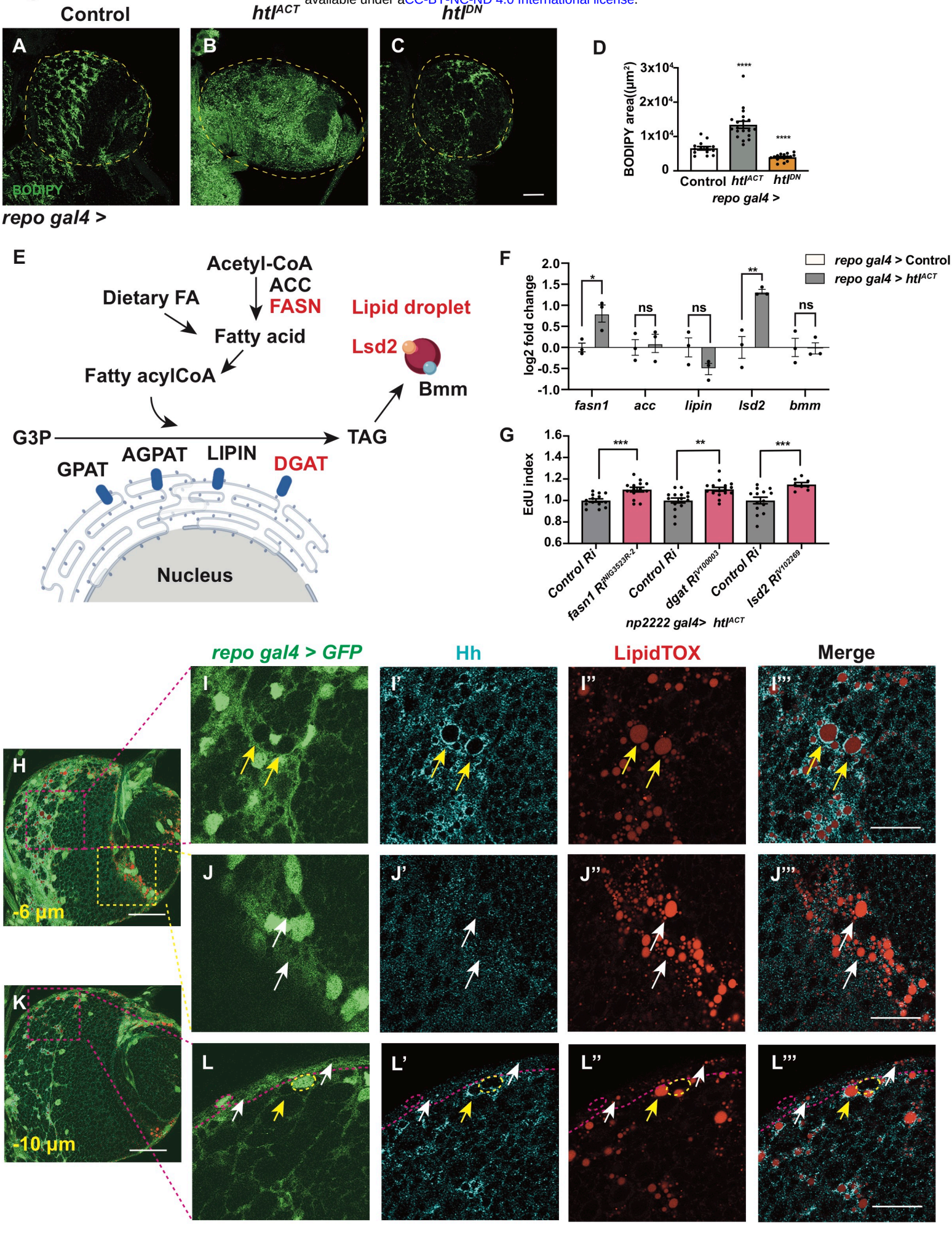

Figure 5

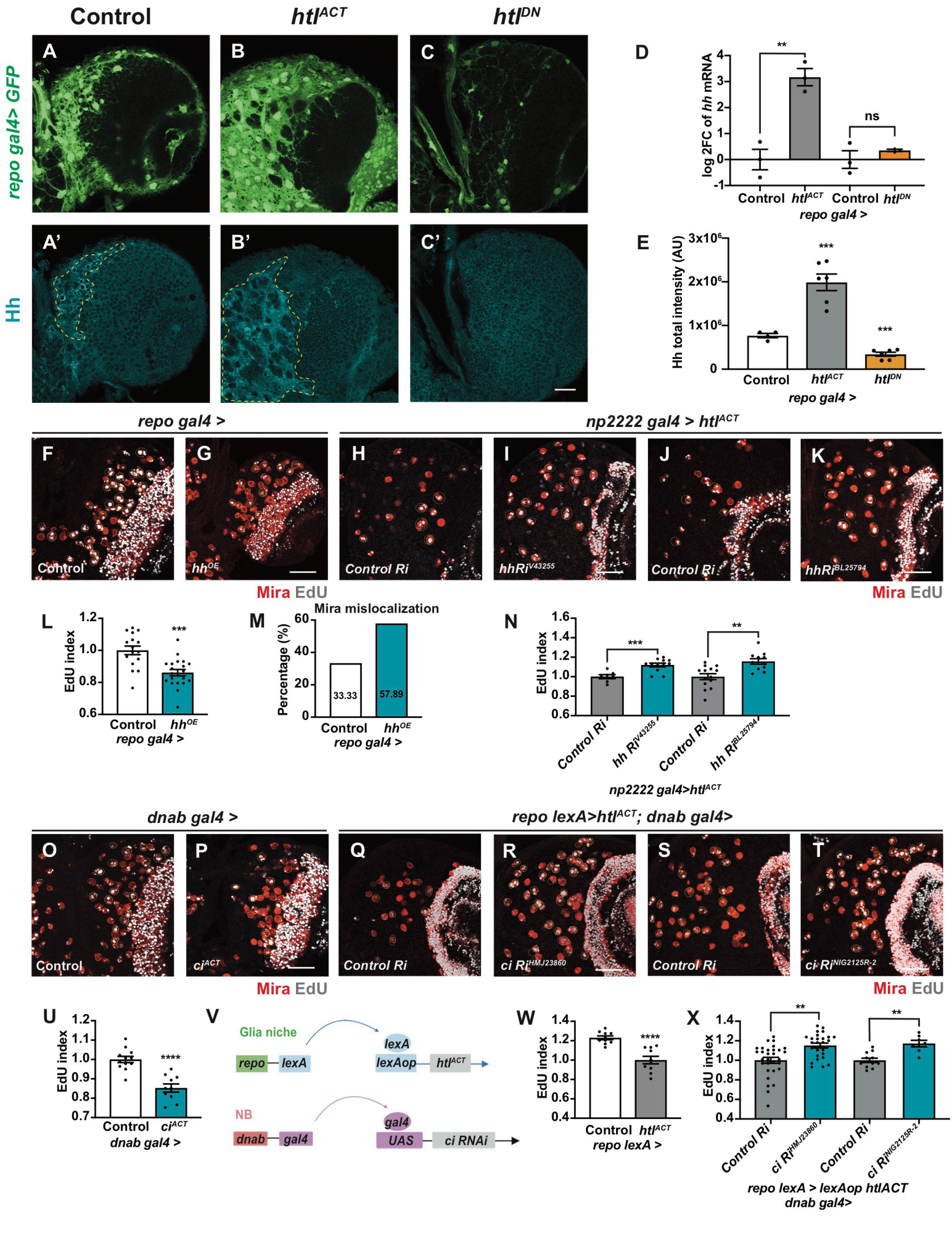

Figure 6

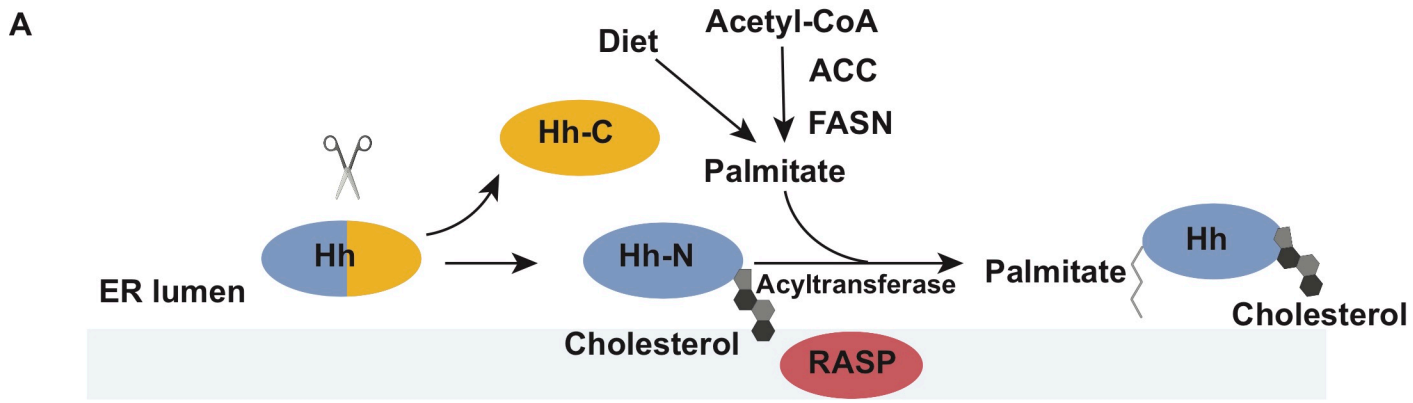

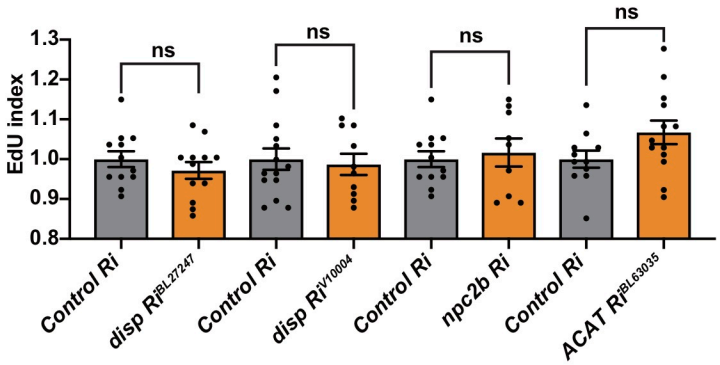

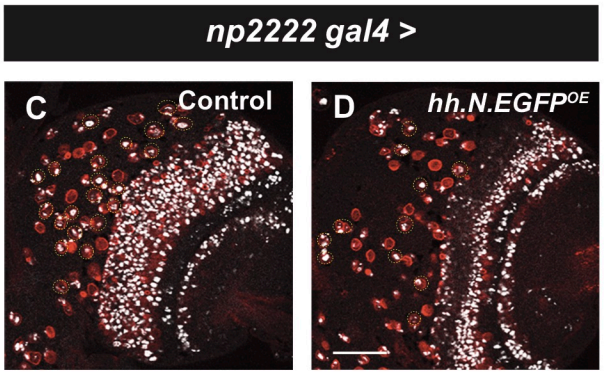

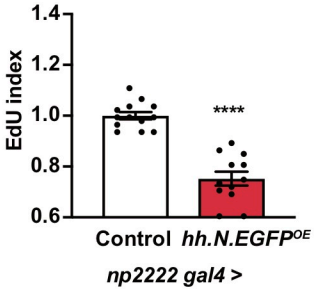

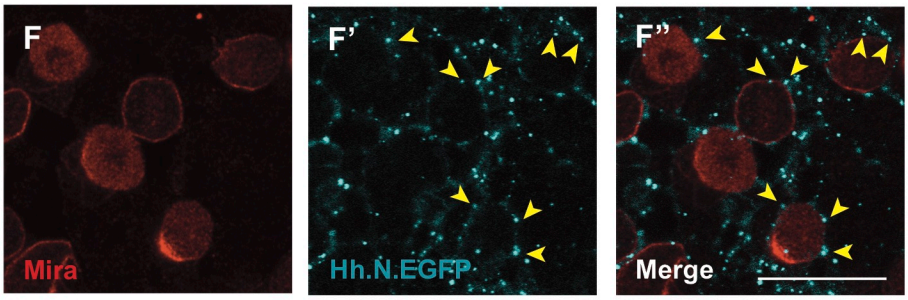

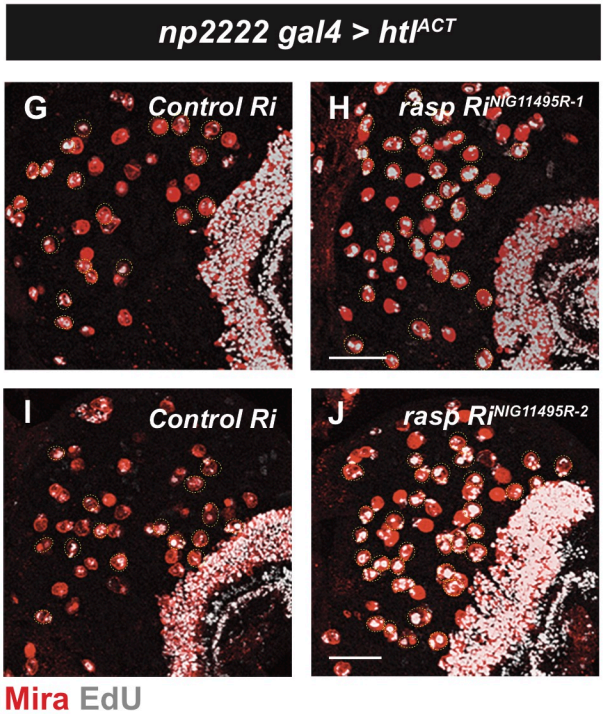

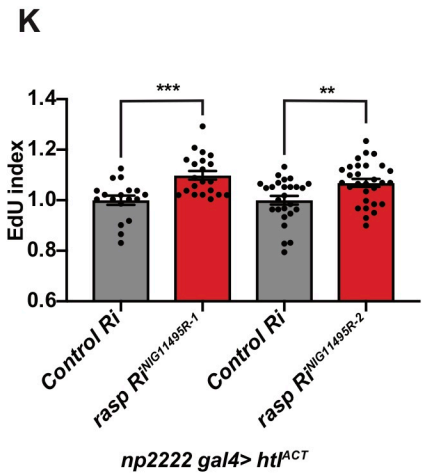

Figure 7